Journal Name

ARTICLE

Deep insight on Zr / Fe combination for successful $Pt/CeO_2/Al_2O_3$ WGS catalyst doping

Received 00th January 20xx,
Accepted 00th January 20xx

DOI: 10.1039/x0xx00000x

www.rsc.org/

M. González-Castaño[a], S. Ivanova[a], T. Ioannides[b], M. A. Centeno[a], J. A. Odriozola[a]

An efficient promotion of the $Pt/CeO_2/Al_2O_3$ catalytic system was achieved by the addition of two different ceria promoters, Zr and Fe. From the exhaustive data analysis, the key features for enhanced catalytic performance and the roles of each doping metal are established. The combination of both doping agents manifests synergistic effect reflected on noteworthy improvements in H_2 reducibility. In addition the catalyst' doping influences its chemisorptive properties, which is reflected in increase of the easiness of carbonaceous species desorption, thus leading to superior catalyst's resistance toward deactivation.

Introduction

A successful implementation of mobile hydrogen technology based on PEM fuel cells needs the development of more efficient water gas shift (WGS) units. The efficiency of these units could be increased either by process intensification with the use of structured catalysts[1] or by development of better catalytic systems. Thereby the catalysts' features become fundamental for the successful application of WGS processors in mobile units. In this context the WGS catalyst must not require pre-reduction procedures, must be non-pyrophoric (contrary to low temperature WGS Cu based catalyst) and tolerant toward exposure on air[2].

The volume reduction that mobile application imposes is probably the most important exigency for the WGS catalytic system. Namely, the WGS unit should operate at high space velocities, low contact times and low temperatures.

Within the existing WGS catalysts the noble metal (NM) based ones have been widely studied for the title process [2–4]. Platinum-based catalysts are especially interesting because their turnover frequency is higher in comparison to other NM [5,6]. The choice of support is also highlighted as a critical [7–9] and Pt/CeO_2 has been described as very promising WGS catalyst [10,11]. The enhanced activity of ceria-supported NM catalysts is frequently attributed to the active role of ceria during the reaction, being not only active phase stabilizer but also participant through structural and electronic catalyst properties promotion. The positive effect of ceria presence is related to oxygen vacancies (Ov) which are constituted via Ce^{4+} to Ce^{3+} redox cycles and also, described as potent actives sites for water dissociations processes[12–15]. Typically, support modifications are undertaken to enhance the positive role of ceria on catalyst performance and to increase the number of ceria' oxygen vacancies enhancing the surface dynamic which is normally associated to easier ceria redox properties and OH/H diffusion processes proceeding from water dissociation and/or H_2 spillover phenomena[15–19]. It has been widely demonstrated that the concentration of oxygen vacancies in ceria can be enhanced by the modification of its structure through doping with different cations, such as Zr [20–22], Fe [23–25] and Eu [26] among others. An optimal effect of the doping agent on the oxygen vacancies formation is often reported for doping metal contents around 10 at. % [27,28]. Suitably modified ceria support should possess low barrier for metal-oxygen transfer, should facilitate CO adsorption by controlled acid base properties and should modulate system easiness to adsorb/desorb the intermediate species during the reaction. A fine equilibrium in acid base and redox properties must be then very helpful to diminish the deactivation of the system when the catalytic activity is negatively influenced either by irreversible ceria reduction or by the surface adsorbed species and active sites hindering. Several studies on the use of Zr as doping agent on the basis of its good thermal stability, ability to decrease ceria sintering [22], and suitable acid-base and redox properties are reported [23,24]. Significant improvement of the catalytic behavior upon addition of Zr in Pt/CeO_2 samples was reported either by increase in surface basicity or by redox properties improvement in the NM support interface [29,30]. Similarly, the support modifications obtained through iron doping are correlated to easier oxygen exchange capacities and promoted electronic properties [14,23,31]. However, when Fe is used as dopant, either decrease [32], increase [33] or even no effect [34] on WGS activity has been also reported. Summarizing the reported studies, one can conclude that the effect of Zr and Fe dopants depends on the preparation method, the nature of present phases and their relative proportion as well as on the doping agent loading [27,35,36]. Actually, the influence of all those features may explain the diversity of conclusions published in several works regarding those systems.

In this context, a careful design of Pt-mixed oxides catalysts is needed for appreciating the role of dopants during the WGS reaction. For this reason, Zr and Fe dopants were chosen in the present paper to promote Pt/CeO_2 activity. In addition, the active components are dispersed on Al_2O_3 support in order to spare costly

[a] Departamento de Química Inorgánica e Instituto de Ciencia de Materiales de Sevilla (ICMS), Centro mixto CSIC-Universidad de Sevilla, Avda. Américo Vespucio 49, 41092 Sevilla, Spain
[b] Foundation for Research and Technology-Hellas (FORTH), Institute of Chemical Engineering Sciences (ICE-HT), Stadiou str. Platani, Patras, Greece

catalyst components. Both doping agents are used separately or in combined manner in order to study their synergism.

Experimental

Four different supports were synthesized, CeO_2/Al_2O_3, $Ce_{0.9}Zr_{0.1}O_2/Al_2O_3$, $Ce_{0.9}Fe_{0.1}O_2/Al_2O_3$ and $Ce_{0.9}Zr_{0.05}Fe_{0.05}O_2/Al_2O_3$. The precursor quantities were calculated to obtain cerium oxide or cerium/promoter mixed oxide loading of 20 wt.% in the final material. The preparation of supports was carried out by incipient wetness impregnation on a high surface ɣ-Al_2O_3 powder (Sasol). The metal oxide precursors were $Ce(NO_3)_3{\cdot}6H_2O$, $Fe(NO_3)_3{\cdot}9H_2O$ and $ZrO(NO_3)_2{\cdot}xH_2O$ (Aldrich). After drying, the solids were calcined at 450°C for 4h. In the adopted nomenclature, the oxygen and the subscripts were omitted. The supports CeO_2/Al_2O_3, $Ce_{0.9}Zr_{0.1}O_2/Al_2O_3$, $Ce_{0.9}Fe_{0.1}O_2/Al_2O_3$ and $Ce_{0.9}Zr_{0.05}Fe_{0.05}O_2/Al_2O_3$ are then labeled CeAl, CeZrAl, CeFeAl and CeZrFeAl, respectively.

The nominal platinum content was 4 wt. %. The platinum deposition was carried out by incipient wetness impregnation using tetrammonium nitrate platinate (Johnson-Matthey) slightly modified by 1M acetic acid. The solids were dried and calcined at 350 ºC for 8h. The resulting samples are called Pt/CeAl, Pt/CeZrAl, Pt/CeFeAl and Pt/CeZrFeAl.

The chemical composition was analyzed by X-ray fluorescence (XRF) in a Panalytical AXIOS PW4400 sequential spectrophotometer using as source of radiation Rh tube.

CO chemisorption studies of metallic dispersion were carried out on Micromeritics Autochem II apparatus. Before chemisorption, every sample was reduced 2 h in H_2 at 350ºC, in the same way as prior the WGS reaction, the absorbed H_2 was desorbed at the same temperature by Ar purging for 30 min. The sample was cooled down to -77 ºC before CO pulsing (20 CO pulses) in order to avoid the support contribution as the CO probe molecules are oxidized at room temperature to CO_2 over ceria based systems. The amount of adsorbed CO useful for the calculation of Pt dispersion was estimated by integration till the respective pulse areas become equal.

Temperature Programed Reduction (TPR) experiments were carried out in a conventional quartz reactor connected to thermal conductivity detector (TCD). A 13X molecular sieve was employed to adsorb the water produced during reduction. The feed gas stream (5%H_2 in Ar) was passed through 50 mg of sample with a flow rate of 50 ml/min. The temperature was raised up to 900ºC with 10ºC/min heating rate.

The TPD experiments were carefully designed in order to obtain clean and similar catalytic surfaces before any gas adsorption or reaction. On first place the catalysts were preheated in inert gas (Ar) then reduced under H_2 and finally, the surface species generated by the reduction were removed by secondary heating in inert atmosphere. Adsorption of CO was carried out at room temperature employing a 1% CO/He mixture at a flow rate of 50 cm3/min until surface saturation, subsequent removal of weakly chemisorbed species under inert flow and then, commencement of TPD.

.

FTIR spectra were recorded by using THERMO NICOLET Avatar 380 FT-IR Spectrophotometer, equipped with a DTGS/KBr detector, and accumulating 128 scans at a spectral resolution of 4 cm^{-1}. The experiments were performed *in situ* using a purpose-made IR cell connected to a conventional vacuum adsorption apparatus with residual pressure lower than 10^{-5} mbar. The experiments consisted of small portions CO absorption till saturation and subsequent desorption by heating.

The catalytic test was performed using 1 g of powder sieved between φ=600-800 μm and placed in tubular stainless steel reactor at atmospheric pressure. All the samples were pretreated at 350ºC for 2h under 10% H_2/N_2 stream. The employed gas mixture is composed of 9 % CO, 11 % CO_2, 30 % H_2O and 50% H_2. The latter was chosen in order to simulate a real stream effluent from ethanol reformer unit. Variation of GHSV was carried out by keeping constant the bed volume (1.5 cm^3) and increasing the total gas flow. Reactants and products concentrations were followed by an ABB gas analyzer for CO, CO_2 and H_2O.

Results and discussion

The chemical composition of the obtained samples is presented in Table 1. Differences on the platinum content of the catalysts were detected, enrichment above nominal is observed for the Pt/CeZrAl and Pt/CeFeAl samples. Nevertheless, the obtained overall support compositions are very close to the nominal values.

The Pt dispersion was calculated by CO chemisorption from the total amount of adsorbed CO. It was assumed that each surface platinum atom chemisorbs only one CO molecule and that Pt particles are cubic with one non-exposed face (Shape Factor = 5). The average Pt crystallite size was estimated by using Spinadel and Boudart method [37]. For all Pt catalysts, the same Pt size was observed of 2.7 nm corresponding to 60% of particles dispersion.

Figure 1a presents the effect of gas hourly space velocity (GHSV) modification on the produced CO conversions at a constant temperature of 280 ºC. Opposite results were obtained: meanwhile the bi-doped Pt/CeZrFeAl sample exhibits greater CO conversion at lower space velocities, the Pt/CeZrAl sample takes advantage at higher ones. Taking into account that Pt/CeZrAl sample, presents also the highest Pt loading, one could consider that the platinum quantity rules the catalytic activity at higher space velocities, becoming the support modifications a secondary feature.

Table 1. Chemical composition of the prepared samples and calculated reducibility percentages (RP) from H_2-TPR experiments.

	Al_2O_3 (wt.%)	CeO_2 (wt.%)	ZrO_2 (wt.%)	Fe_2O_3 (wt.%)	Pt (wt.%)	RP (%)
CeAl	75.3	24.7	---	---	---	76
CeZrAl	80.1	17.7	2.2	---	---	86
CeFeAl	81.4	17.4	---	1.2	---	71
CeZrFeAl	81.0	18.0	0.6	0.4	---	79
Pt/CeAl	72.0	24.2	---	---	3.8	91
Pt/CeZrAl	74.7	18.8	1.6	---	4.9	105
Pt/ CeFeAl	78.3	15.9	---	1.1	4.7	100
Pt/ CeZrFeAl	78.8	16.5	0.5	0.4	3.8	118

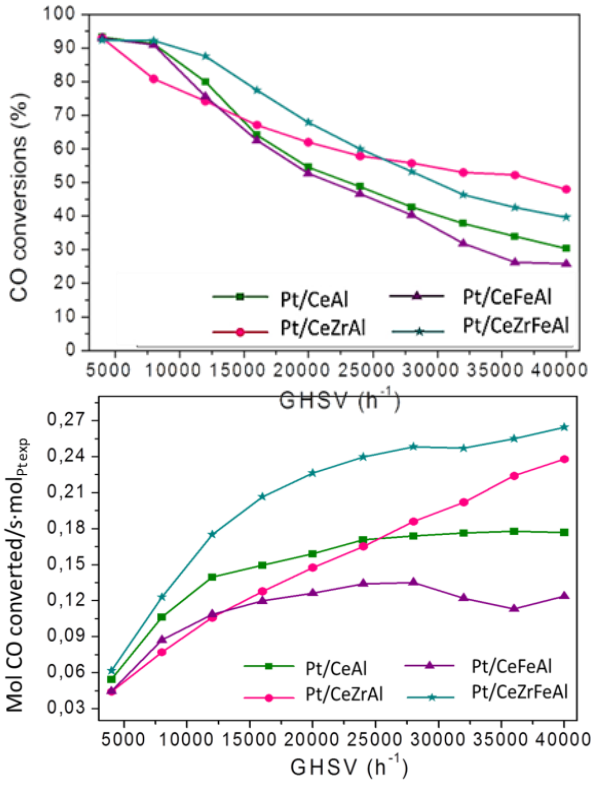

Figure 1. GSHV effect on catalytic activity: a) % CO conversions; b) Normalized activity on exposed Pt atoms

Nevertheless, the support effect can be perceived when the catalytic activity is normalized by the mole of exposed platinum atoms (mol CO converted/s·$mol_{Pt,exp}$) by using the dispersion values calculated from CO chemisorption experiment (Figure 1.b).

Considering the high conversions exhibited for the catalysts on the Figure 1a, the experimental data exposed in Figure 1.b cannot be understood as an actual TOF but rather as normalization to take into account the variations on the Pt content. The bi-doped Pt/CeZrFeAl catalyst shows clearly superior performance at higher GHSV. As the particle size is equivalent and the activity normalization takes into account the number of Pt atoms exposed to the reactants, the observed differences in catalytic activity could be related only to the corresponding support modifications.

The reduction behavior of the samples presented by H_2-TPR profiles are shown in Figure 2, where the supports are compared to their corresponding catalysts. Usually two reduction steps associated with ceria surface and bulk reduction are reported in literature [38,39]. However our CeAl support presents only one wide H_2 consumption and absence of reduction step at higher temperatures, which suggests that either the whole cerium oxide behave as surface ceria or that the bulk fraction reduction step happens above 900 ºC.

Regarding the shape of the profiles, zirconia addition does not provoke any significant modifications. However, the iron doped sample exhibits some differences, due to multiple mixed oxide reduction process occurring simultaneously and to the possible reduction of partially segregated Fe_2O_3 [40]. The shape of CeZrFeAl profile is more similar to that of CeFeAl and hence, the reducibility of the bi-doped CeZrFeAl is ruled by the iron presence. No matter the doping metal, slight shift to lower temperatures of the ceria reduction process is observed, being for CeFeAl and CeZrFeAl supports more significant. These shifts reveal an improvement in reducibility, as reported in our previous studies [35,36] and are probably caused by synergic effect obtained through solid solution formation, in particular, when iron is present.

On the other hand, the catalysts exhibit clearly three differentiated reduction zones (Figure 2a). Two factors have to be taken into consideration when comparing the relative contribution of the reduction processes; the particle size of all reducible species and their interaction within the sample. In general, the temperature of reduction depends on particle size and NM-support interaction [41]. The first H_2 consumption zone takes place up to 250ºC, the second in 250-425 ºC range and the third one above 425 ºC. The observed first zone of

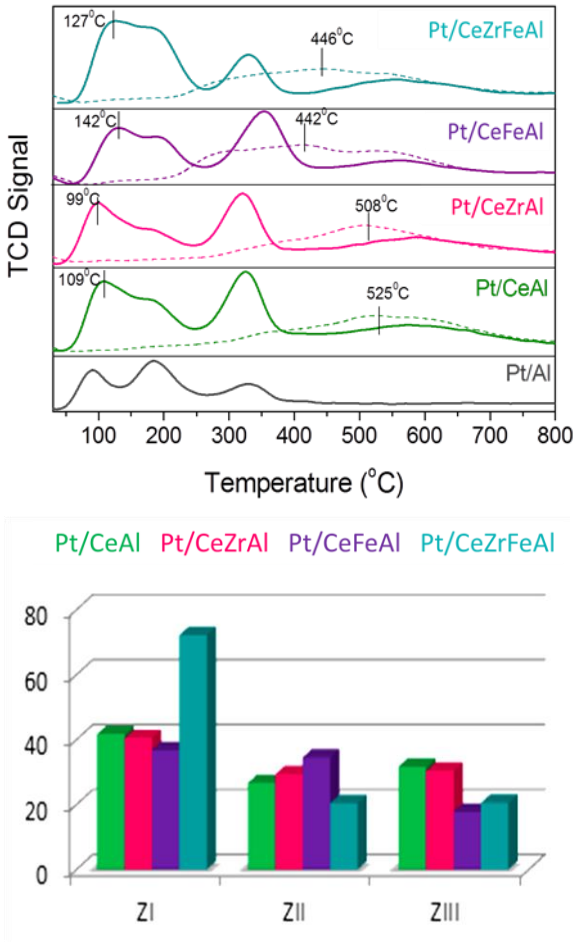

Figure 2. a) H_2-TPR profiles of the supports (dot lines) and their respective catalysts (solid lines); b) Reduction percentage relative to the observed zones of reduction

reduction could be attributed to the reduction of weakly interacting PtO_x species, meanwhile the second to that of PtO_x species strongly interacting with the support. In this zone the proper reduction of the support is also available. The third zone is associated entirely to the support reduction:

As the reduction in this zone occurs at temperatures higher than the maximal WGS reaction temperature (350 ºC) the support will not be completely reduced under reaction conditions [42,43].

The reducibility percentages (RP) calculated comparing the experimental to the theoretical H_2 consumption and considering Pt^{2+}, Fe^{3+} and Ce^{4+} species are listed in Table 1. None of the supports achieve 100% of RP, i.e. complete bulk reduction. However, platinum incorporation leads to superior RP values for all samples. Actually, the platinum samples exhibit RPs closer to 100% being the H_2 overconsumption only noticeable for the Zr-containing samples. This overconsumption can be attributed to the incorporation of hydrogen atoms into the ceria matrix forming H_yCeO_{2-x} bronze like species [44,45]. Fierro et al. [46] reported similar results and concluded that an important amount of hydrogen was incorporated as bronze-like species into the ceria lattice by heating under H_2 at 300 ºC. They related their activity promotion to the quantity of presented H species, (H or OH) in a way that higher the quantity higher the catalyst activity. Our best performing catalyst, Pt/CeZrFeAl shows indeed the highest H_2 overconsumption, in agreement with the results reported in the literature.

The relative H_2 consumption for every temperature zone, i.e. 25-250 ºC, 250-425 ºC and 425-900 ºC is presented in Figure 2b. Taking into account that the distribution cannot be ascribed to particle size effects, it should be the consequence of effects induced by the promoters. Zr lowers the temperature of reduction and Fe entails superior H_2 consumptions. For H_2 reducibility features, similar conclusions for iron promoted Pd-Rh/CeO_2-Al_2O_3 catalyst (TWC) have been proposed[47]. In very good agreement to our results, the iron incorporation to the TWC shifts the noble metals reduction to higher temperatures at the same time that increases the overall H_2 consumption. The observed changes in the noble metals reducibility point out that support composition affects the metal support interaction modifying the electronic structure and the catalyst redox properties [48].

By its part, the Zr and Fe combination results in enhanced relative reduction degree at lower temperature, therefore an excellent redox behavior. It is worthwhile to mention that the main consequence of the easier redox cycles should be a superior OH/H population on the catalyst surface, as suggested by Fierro et al.[46]. Kalamaras et al. [17–19] have noticed catalytic enhancement on doped ceria systems attributed to higher H_2 reducibilitites being associated to enhanced surface dynamics and site reactivities on the Pt particles surroundings. In turn, the support reducibility improvements achieved through Pt incorporation has been related to lower Ce-O energy bond which favors the Ce^{3+}-Ov sites formation. Thus, along Pt-support vicinities the ceria reduction degree (Ce^{3+}-Ov) with the corresponding OH population (generally associated to partially reduced ceria) should be superior. The latter higher capacity to perform redox cycles (implying Ov and OH/H species) should favor the diffusional processes and CO reactions for constituting intermediate species that, in principle, decompose in reaction products.

Interesting results were obtained through combining CO adsorptions followed by FTIR. For that, the samples were pretreated in H_2 at 350 ºC, degassed at 500 ºC in secondary vacuum to clean the surface before the CO adsorption and then the later adsorbed in portions until saturation. At CO saturation, all samples present the same behavior (Figure 3) with the appearance of the Pt^0-CO band at 2100 cm^{-1} indicating the presence of fully reduced Pt after H_2 pretreatment. Furthermore, several other species are observed in the 1800-1100 cm^{-1} region and in the hydroxyl region (3500-3200 cm^{-1}). It should be noted that the bands in the former region, ascribed to carbonaceous species, increased more rapidly than the Pt-CO stretching band. The bands placed at 1650, 1611, 1434, 1397, 1229 and 1219 cm^{-1} could be attributed to different kinds of hydrogen-carbonates, being also discerned its corresponding υ(OH) stretching vibrations at 3617 cm^{-1} [49–51]. The bands situated at 1630 and 1550 cm^{-1} corresponds to carbonates species and bands placed at 1840 cm^{-1} are usually related to bridged carbonyls [52] but also attributed to bridged carbonates [13].

It is usually accepted for the WGS reaction on Pt based catalysts, that CO is absorbed and activated on Pt particles and once activated can directly react with an adjacent O available from the support towards $CO_{2(g)}$, namely redox pathway[53]. However, it is also plausible that the CO species, once activated on metal surfaces, diffuse to the adjacent to Pt support area where oxidation reactions will happen. So, the CO molecules should react with OH/H species towards

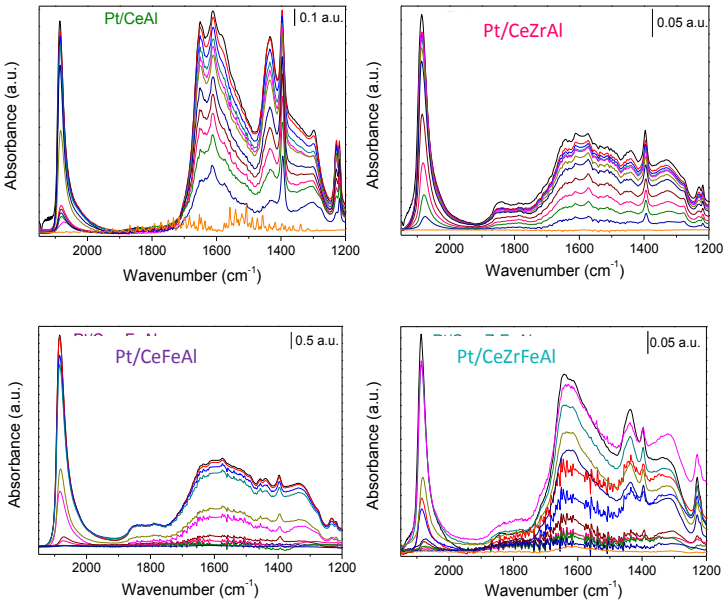

Figure3. FTIR spectra obtained during CO adsorption on the catalysts

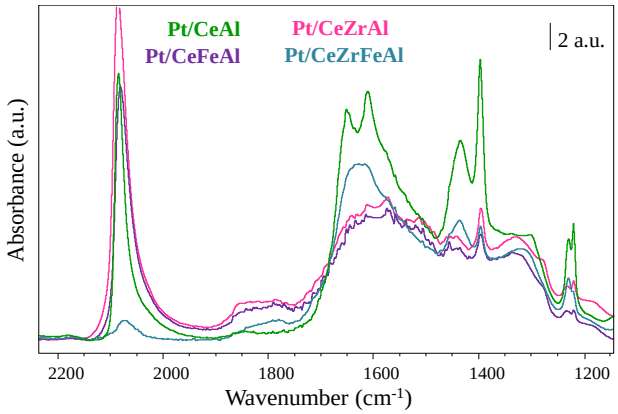

Figure 4. Comparison of CO adsorption spectra at 1.4 µmol CO coverage

reaction intermediates and then, CO_2[54,55]. In any case, subsequent CO_2 reactions with O/OH surface species developing carbonates or hydrogen-carbonates on the support are also plausible. In this way, the CO species could be transferred from Pt to the support producing carbonaceous species[56,57].

Regarding the studied samples significant differences in terms of band relative intensity are observed at low CO coverage (1.4µmol), spectra presented in Figure 4. These differences can be indirectly correlated to the catalyst' capacity to activate CO molecules

and to transfer them to the support by reacting either with O or with OH/H species. Within the studied samples, the bi-doped sample Pt/CeZrFeAl shows higher capacity to transfer CO species to the support, confirmed by the lowest intensity of its corresponding Pt-CO band (at 2086 cm^{-1}) and the resulting important relative intensity of carbonaceous species bands in the 1800-1100 cm^{-1} region.

So, the superior amount of carbonate like species developed on the support should imply enhanced oxidation reactions with O species to CO_2 and then, to $CO_3^=$ but also with OH/H for developing hydrogen-carbonate like species. This feature could be also related to the greater H_2 reducibility exhibited by the Pt/CeZrFeAl sample during the H_2-TPR experiments. In fact, the observed superior capacity for diffusing H species through the lattice should be allowed by faster reversible Ce^{4+}/Ce^{3+} - Ov interconversions. Therefore, the support modifications lead to boosted surface dynamics favoring either the Ov constitution as the OH/H species (Scheme 1). Thus, the diffusional and redox enhancement on the Pt/CeZrFeAl accounts for the easier transfer and reaction of CO species resulting on larger amounts of carbonates and bicarbonates species developed on the support.

Particular attention should be paid on adsorbed carbonaceous species and their desorption behavior, as they can potentially

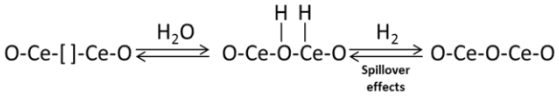

Scheme 1: Simplified hydrogen surface dynamics.

deactivate the catalyst by blocking its active sites [58,59]. In this context, the TPD-TPO characterization technique could provide useful information related to the easiness of carbonaceous species desorption. The TPD profiles of CO_2, H_2 and CO registered during desorption step after CO adsorption at room temperature are presented in Figure 5.

For all catalysts, two CO (signal m/z=28) desorption zones are observed, being 250 ºC the zone separation temperature. A difference in the relative desorbed CO amounts is identified, with the highest quantity observed for the Pt/CeZrAl anPt/CeFeAl samples. Comparable TPD profiles for similar catalysts could be found in the literature [13, 47-49]. For example, Du et al. [13] report weakly interacting CO species desorbing at temperatures below 100 ºC and strongly interacting species evolving at around 320 ºC. Chemisorbed CO molecules of intermediate strength desorbing in the 170 - 260 ºC region are observed for all catalysts, except for the Pt/CeZrFeAl system. The accompanying CO_2 and H_2 desorption profiles are also rather complex. Pt/CeAl, Pt/CeZrAl and Pt/CeFeAl samples show comparable CO_2 profiles with wide desorption process starting at 300 ºC up to the highest experiment temperature. Simultaneously, H_2 species are evolved in the same temperature range. Simultaneous CO_2 and H_2 desorption is related to formate decomposition [50]. Considering that, the surface was pre-cleaned before and after the reduction treatment, the catalytic surface should be devoid of hydrogen species. The observed CO_2 then can only be formed through the reaction of adsorbed CO with OH species on the catalyst surface. Only the sample Pt/CeZrFeAl shows clear differentiation in its TPD profiles compared to the other samples. CO_2 and H_2 profiles do not coincide with their respective desorption peaks centered respectively at around

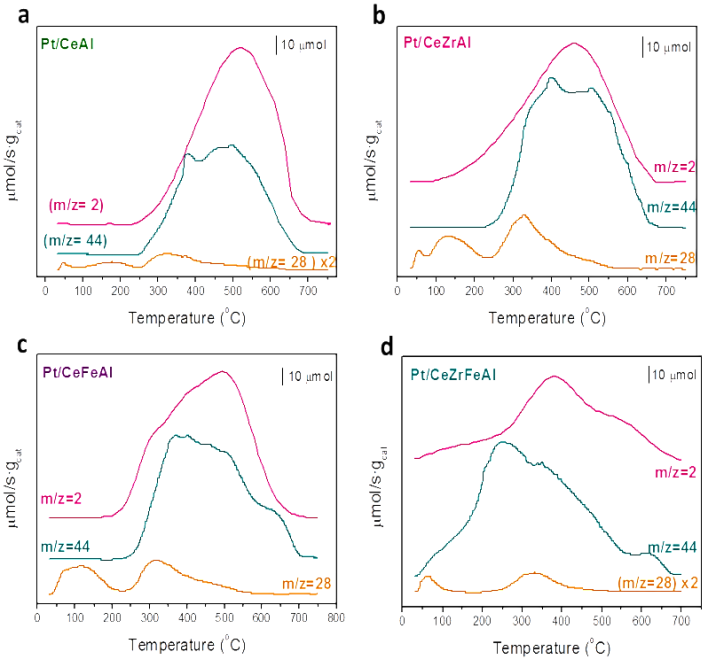

Figure 5. CO-TPD obtained for a) Pt/CeAl; b) Pt/CeZrAl; c) Pt/CeFeAl and d) Pt/CeZrFeAl

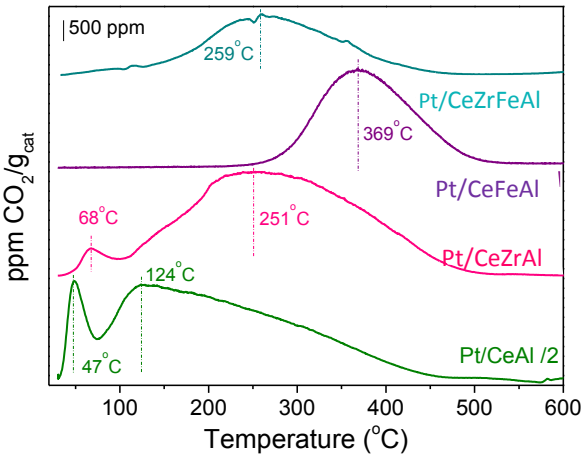

Figure 6. TPO obtained after the CO-TPD experiment

240 ºC and 370 ºC. Mullins et al. [47] attributed the CO_2 desorption at temperatures below 127 ºC to the reaction of adsorbed CO with oxygen species on metallic Pt sites.

Considering the excellent reducibility of this sample, this low temperature CO_2 formation is probably due either to the oxidation of the adsorbed CO with lattice oxygen or to Boudouard reaction. If the later reaction occurs, residual carbon on the catalyst surface during the CO-TPD experiment should be formed and easily titrated by a TPO run. CO_2 produced during TPO is presented in Figure 6. The profiles differ considerably among the examined catalysts. The Pt/CeAl sample CO_2 profile intensity is reduced by half in order to compare it to the others. The important CO_2 intensity in this case indicates that the introduction of doping agents lead to decrease of the overall C deposits in respect to the unpromoted sample. This effect also specifies that ceria doping results in more labile carbonaceous species on the catalyst surface, species more readily desorbed in TPD conditions. On the other hand, Pt/CeAl and Pt/CeZrAl systems exhibit two different desorption processes, where the lower temperature desorption is significantly less important than that at higher temperature. In both cases the CO_2 desorption process begins at lower temperatures compared to those for Fe-containing samples. The Pt/CeFeAl and Pt/CeZrFeAl samples, however presents lower C deposit quantity which is oxidized to CO_2 in higher temperature zones centered at 369 ºC and 259 ºC respectively.

Goguet et al. [51] reported DRIFT studies of the adsorbed species after CO adsorption. They observed that the species associated to the deactivation are generally formates and carbonates, and that they are not affected by the exposure time and are desorbed at low temperature (up to 250 ºC) in the presence of oxygen. At room temperature, the oxidation products proceeds from adsorbed carbonyl species meanwhile at higher temperature, (260-290 ºC) CO_2 species originates from the oxidation of carbon deposits. It was also reported that the carbon deposits quantity varies with CO exposure time, indicating a continuous accumulation of carbon able of being oxidized. The carbon depositions on noble metal of the X group are well known as cause of deactivation. The formation of carbon deposits in the presence of CO could be ascribed to the Boudouard's reaction (2 CO $\rightarrow$C+CO_2). Some works relates the carbon deposit formation to the platinum species and to the oxygen vacancies (Ce^{3+} population) [52,53]. Holmgren et al. [11,49] reported that the CO disproportionation occurs on oxygen vacancies, but important carbon deposits were set up when ceria catalysts are promoted with platinum. Then, although the CO dissociation happens on the support surface, carbon species can migrate from the support to metallic platinum constructing carbon rings around the Pt particles.

Therefore, it can be assumed that both carbonaceous species (i.e. carbonates, formates) and carbon deposits remain on the catalyst surface after the CO-TPD. Our TPO results show a decrease of the carbonaceous and carbon deposits with the addition of doping agents. Moreover, the carbonaceous species appearing under 250 ºC are not observed for the iron promoted samples exhibiting a decrement of the total desorbed species amount. Therefore, the iron presence appears to enhance the decomposition rate of those species, thus lowering the rate of catalyst's deactivation. On the other hand, the Pt/CeFeAl shows increased remaining species stability, confirmed by the highest oxidation temperature observed in its TPO profile.

When both dopants are combined, the beneficial effects are maintained. The iron presence results in diminishing quantities of the remaining species. Besides the lower quantities, it appears that the species stability is ruled out by the zirconia presence, higher the Zr concentration, lower the temperature of oxidation (the desorption edge for Pt/CeZrFeAl shifts to lower temperatures in respect to the Pt/CeFeAl).

The quantification of the desorbed species could be also performed assuming that CO desorb without reaction during the CO-TPD experiments or as CO_2 reacted through i) $(CO + [O]_s \rightarrow CO_2)$; ii) $(CO + [OH]_s \rightarrow {}^1/_2\, H_2 + CO_2)$ and iii) $(2CO \rightarrow C + CO_2)$ where the subscript "s" indicates that proceed from the support.

On the other hand and regarding to the TPO post CO-TPD, the CO_2 species desorbed should proceed from: i) intermediate species not desorbed along CO-TPD experiments or ii) carbon deposits produced through the Boudouard's reaction.

Table 2 shows the relative CO reactivity on all those processes. The $CO_{OH,S}$ species account for the CO species that, during the CO-TPD, react with the support-contained OH species. These

Table 2. Table 2. Relative proportion of the occurring interactions calculated after TPD-TPO

	% CO_{OH}	% $CO_{[o]sup}$	% CO_{total}	% CO_{deact}
Pt/CeAl	17.31	45.08	62.39	37.61
Pt/CeZrAl	18.45	53.36	71.81	28.18
Pt/CeFeAl	26.56	55.10	81.66	18.34
Pt/CeZrFeAl	25.00	57.00	82.00	18.00

species are calculated from the observed H_2 amount. The difference between the total reacted CO (CO_{total}) and the $CO_{OH,S}$ species account for the CO reacting to the O species of the support, $CO_{O,S}$. According to the TPO run, no matter the origin of the CO_2 species, it can be assumed that those species are potentially responsible for the deactivation processes on the catalyst surface. Then, the overall CO_2 species detected during the TPO could be directly related to the potentially deactivator CO fraction, CO_{deact}.

Apparently, all doping agents promote CO to CO_2 oxidation in comparison to the unpromoted sample. The promotion depends on the doping metal, as for example, iron presence boosts the CO reactivity via OH. In the same time, an enhance of the O species mobility occurs (reaction through support`s O species) no matter the doping agent.

In addition, important improvements concerning the deactivation species formation are achieved when both doping metals are added to the ceria matrix. While zirconia addition helps the rapid evacuation of the species susceptible to deactivate the catalysts from the surface, the iron incorporation significantly diminish their concentration. Also the stability of the deactivation species decreases considerably, being ruled by the zirconia presence.

Conclusions

The combination of both Fe and Zr dopants results in finely balanced promoted system. Important synergistic effect was confirmed by the greater H_2 consumption at lower temperatures and significant overconsumption suggesting enhanced H surface dynamics related to boosted redox cycles and Ce^{3+}- Ov active sites. The latter invokes greater concentration and mobility of the H species (OH and H species) for the bi-doped sample. Therefore, the combination of Zr and Fe results in easier CO reactions on catalyst' surface, confirmed by FTIR and CO-TPD experiments and, hence superior reaction rates at high GHSV.

In addition, Zr and Fe combination enhances catalyst' resistance toward carbon deposits, being Fe identified as the most potent inhibitor and Zr responsible for the easiness of carbonaceous species desorption.

In conclusion, the enhanced catalytic performance of the Pt/CeZrFeAl appears to be a conjunction of greater reducibility linked to enhanced capacity to develop surface carbonates like species that, besides, decompose easily to reaction products. As a consequence, the combination of both promoters allows not just better catalytic activity but also higher resistance towards deactivation effects.

References

1 R. J. Farrauto, Y. Liu, W. Ruettinger, O. Ilinich, L. Shore and T. Giroux, *Catal. Rev.*, 2007, **49**, 141–196.

2 C. Ratnasamy and J. P. Wagner, *Catal. Rev.*, 2009, **51**, 325–440.

3 D. Andreeva, V. Idakiev, T. Tabakova, A. Andreev and R. Giovanoli, *Appl. Catal. A Gen.*, 1996, **134**, 275–283.

4 T. Tabakova, V. Idakiev, D. Andreeva and I. Mitov, *Appl. Catal. A Gen.*, 2000, **202**, 91–97.

5 P. Panagiotopoulou and D. I. Kondarides, *Catal. Today*, 2006, **112**, 49–52.

6 G. G. Olympiou, C. M. Kalamaras, C. D. Zeinalipour-Yazdi and A. M. Efstathiou, *Catal. Today*, 2007, **127**, 304–318.

7 A. Trovarelli, *Catal. Rev.*, 1996, **38**, 439–520.

8 T. Tabakova, L. Ilieva, I. Ivanov, R. Zanella, J. W. Sobczak, W. Lisowski, Z. Kaszkur and D. Andreeva, *Appl. Catal. B Environ.*, 2013, **136–137**, 70–80.

9 C. M. Kalamaras, I. D. Gonzalez, M. Navarro, L. G. Fierro and A. M. Efstathiou, 2011, 11595–11610.

10 G. Jacobs, U. M. Graham, E. Chenu, P. M. Patterson, A. Dozier and B. H. Davis, *J. Catal.*, 2005, **229**, 499–512.

11 D. Tibiletti, A. Amieiro-Fonseca, R. Burch, Y. Chen, J. M. Fisher, A. Goguet, C. Hardacre, P. Hu and D. Thompsett, *J. Phys. Chem. B*, 2005, **109**, 22553–22559.

12 T. R. Reina, S. Ivanova, J. J. Delgado, I. Ivanov, V. Idakiev, T. Tabakova, M. A. Centeno and J. A. Odriozola, *ChemCatChem*, 2014, **6**, 1401–1409.

13 A. Holmgren, B. Andersson and D. Duprez, *Appl. Catal. B Environ.*, 1999, **22**, 215–230.

14 M. González Castaño, T. R. Reina, S. Ivanova, M. A. Centeno and J. A. Odriozola, *J. Catal.*, 2014, **314**, 1–9.

15 M. González-Castaño, S. Ivanova, O. H. Laguna, L. M. Martínez T., M. A. Centeno and J. A. Odriozola, *Appl. Catal. B Environ.*, 2017, **200**, 420–427.

16 M. A. Centeno, M. Paulis, M. Montes and J. A. Odriozola, *Appl. Catal. A Gen.*, 2002, **234**, 65–78.

17 C. M. Kalamaras, D. D. Dionysiou and A. M. Efstathiou, *ACS Catal.*, 2012, **2**, 2729–2742.

18 C. M. Kalamaras, K. C. Petallidou and A. M. Efstathiou, *Appl. Catal. B Environ.*, 2013, **136–137**, 225–238.

19 K. C. Petallidou, C. M. Kalamaras and A. M. Efstathiou, *Catal. Today*, 2014, **228**, 183–193.

20 X. Du, D. Gao, Z. Yuan, N. Liu, C. Zhang and S. Wang, *Int. J. Hydrogen Energy*, 2008, **33**, 3710–3718.

21 S. Damyanova, B. Pawelec, K. Arishtirova, M. V. M. Huerta and J. L. G. Fierro, *Appl. Catal. B Environ.*, 2009, **89**, 149–159.

22 A. Martinez-Arias, M. Fernández-García, A. B. Hungria, A. Iglesias-Juez, O. Gálvez, J. A. Anderson, J. C. Conesa, J. Soria and G. Munuera, *J. Catal.*, 2003, **214**, 261–272.

23 T. R. Reina, S. Ivanova, V. Idakiev, J. J. Delgado, I. Ivanov, T. Tabakova, M. A. Centeno and J. A. Odriozola, *Catal. Sci. Technol.*, 2013, **3**, 779.

24 M. González-Castaño, T. R. Reina, S. Ivanova, L. M. Martínez Tejada, M. A. Centeno and J. A. Odriozola, *Appl. Catal. B Environ.*, 2016, **185**, 337–343.

25 L. Ilieva, T. Tabakova, G. Pantaleo, I. Ivanov, R. Zanella, D. Paneva, N. Velinov, J. W. Sobczak, W. Lisowski, G. Avdeev and A. M. Venezia, *Appl. Catal. A Gen.*, 2013, **467**, 76–90.

26 W. Y. Herna, M. A. Centeno, F. Romero-sarria, J. A. Odriozola and A. V Ame, 2009, 5629–5635.

27 O. H. Laguna, M. A. Centeno, M. Boutonnet and J. A. Odriozola, *Appl. Catal. B Environ.*, 2011, **106**, 621–629.

28 H. Bao, X. Chen, J. Fang, Z. Jiang and W. Huang, *Catal. Letters*, 2008, **125**, 160–167.

29 S. Ricote, G. Jacobs, M. Milling, Y. Ji, P. M. Patterson and B. H. Davis, *Appl. Catal. A Gen.*, 2006, **303**, 35–47.

30 A. M. Duarte de Farias, D. Nguyen-Thanh and M. A. Fraga, *Appl. Catal. B Environ.*, 2010, **93**, 250–258.

31 M. Lo, M. Ojeda, P. Terreros, S. Rojas, T. Herranz, J. L. G. Fierro, M. Curie, M. Gracia and J. R. Gancedo, *Chem. Mater.*, 2005, 2329–2339.

32 T. Dhannia, S. Jayalekshmi, M. C. Santhosh Kumar, T. Prasada Rao and a. Chandra Bose, *J. Phys. Chem. Solids*, 2010, **71**, 1020–1025.

33 P. C. A. Brito, D. A. A. Santos, J. G. S. Duque and M. A. Macêdo, *Phys. B Condens. Matter*, 2010, **405**, 1821–1825.

34 L. Yue and X. M. Zhang, *J. Alloys Compd.*, 2009, **475**, 702–705.

35 S. Damyanova, B. Pawelec, K. Arishtirova, M. V. M. Huerta and J. L. G. Fierro, *Appl. Catal. A Gen.*, 2008, **337**, 86–96.

36 T. R. Reina, E. Papadopoulou, S. Palma, S. Ivanova, M. a. Centeno, T. Ioannides and J. a. Odriozola, *Appl. Catal. B Environ.*, 2014, **150–151**, 554–563.

37 L. Spenadel and M. Boudart, *J. Phys. Chem.*, 1960, **64**, 204–207.

38 G. Balducci, P. Fornasiero, R. Di Monte, J. Kaspar, S. Meriani and M. Graziani, *Catal. Letters*, 1995, **33**, 193–200.

39 H. Vidal, J. Kašpar, M. Pijolat, G. Colon, S. Bernal, A. Cordón, V. Perrichon and F. Fally, *Appl. Catal. B Environ.*, 2001, **30**, 75–85.

40 P. Arnoldy, A. Moulijn and O. J. Wimmers, *J. Phys. Chem*, 1986, **90**, 1331–1337.

41 M. J. Tiernan and O. E. Finlayson, *Appl. Catal. B Environ.*, 1998, **19**, 23–35.

42 S. Damyanova, C. A. Perez, M. Schmal and J. M. C. Bueno, *Appl. Catal. A Gen.*, 2002, **234**, 271–282.

43 T. Yamaguchi, *J. Catal.*, 1981, **67**, 324–330.

44 D. Andreeva, I. Ivanov, L. Ilieva and M. V. Abrashev, *Appl. Catal. A Gen.*, 2006, **302**, 127–132.

45 O. T. A. Laachir, V. Perrichon, A. Badri, J. Lamotte, E.Catherine, J.C.Lavalley, J. El Fallah, L. Hilaire, F. le Normand, E. Quéméré, G. N. Sauvion, *J. Chem. Soc. Faraday Trans.,* 1991, **87**, 1601–1609.

46 J. L. G. Fierro, J. Soria, J. Sanz and J. M. Rojo, *J. Solid State Chem.*, 1987, **66**, 154–162.

47 P. S. Lambrou and A. M. Efstathiou, *J. Catal.*, 2006, **240**, 182–193.

48 S. J. Tauster, S. C. Fung, R. T. Baker and J. A. Horsley, *Science*, 1981, **211**, 1121–1125.

49 C. Binet, M. Daturi and J.-C. Lavalley, *Catal. Today*, 1999, **50**, 207–225.

50 C. M. Kalamaras, S. Americanou and A. M. Efstathiou, *J. Catal.*, 2011, **279**, 287–300.

51 G. Jacobs, P. M. Patterson, U. M. Graham, D. E. Sparks and B. H. Davis, *Appl. Catal. A Gen.*, 2004, **269**, 63–73.

52 P. Bazin, O. Saur, J. C. Lavalley, M. Daturi and G. Blanchard, *Phys. Chem. Chem. Phys.*, 2005, **7**, 187–194.

53 T. P. H. E. F. Armstrong, *Proc. R. Soc. London*, 1920, **A97**, p.265.

54 R. Burch, *Phys. Chem. Chem. Phys.*, 2006, **8**, 5483–500.

55 T. Shido and Y. Iwasawa, *J. Catal.*, 1993, 141, 71–81.

56 a. a. Phatak, N. Koryabkina, S. Rai, J. L. Ratts, W. Ruettinger, R. J. Farrauto, G. E. Blau, W. N. Delgass and F. H. Ribeiro, *Catal. Today*, 2007, **123**, 224–234.

57 W. Ruettinger, X. Liu and R. J. Farrauto, *Appl. Catal. B Environ.*, 2006, **65**, 135–141.

58 A. Goguet, F. Meunier, J. P. Breen, R. Burch, M. I. Petch and A. Faur Ghenciu, *J. Catal.*, 2004, **226**, 382–392.

59 M. M. Schubert, A. Venugopal, M. J. Kahlich, V. Plzak and R. J. Behm, *J. Catal.*, 2004, **222**, 32–40.